Proceedings of Fifth International Conference on **Enhanced, Compact and Ultra-Compact Heat Exchangers: Science, Engineering and Technology**, Eds. R.K. Shah, M. Ishizuka, T.M. Rudy, and V.V. Wadekar, Engineering Conferences International, Hoboken, NJ, USA, September 2005.

CHE2005 – 34

AN EXPERIMENTAL STUDY OF LOUVER-FIN FLAT-TUBE HEAT EXCHANGER PERFORMANCE UNDER FROSTING CONDITIONS

Yongfang Zhong, Anthony M. Jacobi*

University of Illinois at Urbana-Champaign, Urbana, IL, USA
Department of Mechanical and Industrial Engineering; yzhong1@uiuc.edu
* Department of Mechanical and Industrial Engineering; a-jacobi@uiuc.edu

ABSTRACT

The louver-fin flat-tube heat exchanger is recognized for compactness and high air-side heat transfer coefficient, but few studies have been reported on its performance under frosting conditions. In order to extend its application, an experimental study on the thermal-hydraulic performance of louver-fin flat-tube heat exchangers was conducted over a wide range of frosting conditions to examine the effects of geometric and environmental parameters. The results show that frost accumulation is a strong function of the operating conditions, while the pressure drop behavior is dominated by the geometry of the heat exchanger. Under the same operating conditions, the ratio of the pressure drop during frost growth to the initial pressure drop without frost deposition was found to be identical for heat exchangers with equal flow depth. Different trends for heat transfer coefficients during frost growth are found for heat exchangers with different geometries. The effects of parameters such as fin pitch, air flow depth, air humidity, coolant temperature, and air flow rate are discussed. Design issues for louver-fin flat-tube heat exchangers in frosting application are discussed.

NOMENCLATURE

A_{tot}=total air-side heat transfer area (mm^2)
C_p=specific heat at constant pressure (kJ/kg-K)
F=the correction factor for cross flow
Q=heat transfer rate (kW)
m=frost accumulation (kg)
$\dot{m}$ =frost accumulation per second (kg/second)
i =specific enthalpy (kJ/kg)
T= temperature (□)
ω =humidity ratio (kg/kg-dry air)
U=overall air-side heat transfer coefficient including conduction in the frost layer and convection between the frost surface and the air (kW/m^2-K)
LMTD= log-mean temperature difference (□)
F_p=fin pitch (mm)
L_p=louver pitch (mm)
H=length of the test specimen (mm)
W= width of the test specimen (mm)
D=depth of the test specimen (mm)
Tw=tube width (mm)
Td=tube depth (mm)
Fl=fin length (mm)
δ =fin thickness (m)
δ_t =tube wall thickness (mm)
α =louver angle (°)

INTRODUCTION

Flat-tube, louver-fin heat exchangers are constructed by brazing aluminum fins to extruded aluminum flat tubes with microchannels. Flat-tube heat exchangers have inherent advantages over round-tube heat exchangers: for example, the flat-tube geometry provides higher fin efficiency than the round-tube geometry, and the wake region behind the flat tube does not reduce heat transfer on the downstream fin regions (Webb 1994). Because of the advantages of this configuration, flat-tube heat exchangers have been widely used in the automotive industry for decades, and a lot of research has been recently directed towards replacing round-tube heat exchangers in a broad range of other applications.

While the flat-tube heat exchanger has drawn significant attention as a replacement for the round-tube

heat exchanger, few studies of the thermal-hydraulic performance of full-scale louver-fin, flat-tube heat exchangers under frosting conditions have appeared in the open literature. Kim and Groll (Kim *et al*, 2003)studied louver-fin, flat-tube heat exchangers to replace spine-fin, round-tube heat exchangers with the same heat capacity in a unitary split system as the outdoor coil for air-conditioning and heat pumping applications. Nevertheless, their study was restricted to systemic performance. Detailed information on airside thermal-hydraulic performance and frost accumulation rates on flat-tube heat exchangers was not available in their paper.

Xia and co-workers (Xia *et al*, 2004) presented pressure drop and heat transfer data for three louver-fin, flat-tube heat exchangers during frost growth, with fixed inlet air temperature, humidity, blower frequency, coolant temperature and mass flow rate. They concluded that during frost growth the heat transfer coefficient decreased and the pressure drop increased. Unfortunately, they used a frost conductivity correlation developed for substrate and air temperatures different from their experimental conditions (Lee *et al*, 1997). Furthermore, the model they used to predict frost thickness did not account for densification, and their experimental approach assumes a uniform thickness. These methods may be inadequate to obtain a detailed description of frost distribution, and the experiments were restricted to a very narrow range, limiting their generality.

Xia and co-workers (Xia *et al*, 2004) studied louver-fin flat-tube heat exchangers under the frost/defrost conditions. Constant periods were chosen in their experiments for the frost and defrost cycle: one-hour frost growth, followed by a 4 to 5-minute defrost. The length of the frost cycle was arbitrary, and the length of the defrost was sufficient to melt all frost. Each frost cycle was conducted under fixed environmental conditions, but among the sequential frost cycles the air temperature had a variation of 3 □ and relative humidity had a variation of 10%. They concluded that the total frost mass on the heat exchangers at the end of each frost cycle had little variation after the third or fourth cycle, and that the droplets from defrost have significant effects on pressure drop and heat transfer. The specimens they used had different fin geometrics and manifold arrangements, and these geometric differences can have a profound impact on water drainage (Joardar *et al*, 2004). For these reasons, only very limited conclusions about geometric effects on frosting, defrosting, and refrosting can be drawn from this work.

Little work has been done on geometric and environmental effects of louver-fin flat-tube heat exchangers under frosting conditions, and the extant experimental data are inadequate to obtain a generalized understanding of the performance of these heat exchangers. The purpose of the research reported here is to explore the geometric effects of flat-tube heat exchanger on thermal-hydraulic performance and to explore the influence of different operating parameters on the performance of such heat exchangers under frosting conditions. In this paper, experimental results are reported for frost accumulation, pressure drop and overall heat transfer coefficient. The parameters governing the performance during frost growth, such as fin pitch, air temperature and humidity, and coolant temperature are analyzed and discussed. The results may provide design guidance for engineers and will add to the growing experimental basis for understanding flat-tube heat exchanger performance under frosting conditions.

METHOD

Experimental Apparatus and Test Conditions

An experimental apparatus consisting of an environmental chamber, a wind tunnel with a heat exchanger test section, a coolant supply system, and a data acquisition system was constructed to test the full-scale flat-tube heat exchangers under frosting conditions. The wind tunnel was placed inside the environmental chamber which provided conditioned air at a desired temperature and humidity. Performance of the heat exchangers under frosting conditions was studied experimentally using this apparatus under fixed upstream air temperature and relative humidity, air flow rate, coolant flow rate and coolant inlet temperature.

All the specimens, which have the same tube configuration and manifolds at the top and bottom, were made of aluminum louver fins brazed on flat plain aluminum tubes. Geometric specifications for the test specimens are provided in Table 1. Experimental conditions are summarized in Table 2. Condition A, under which specimens 1 and 2 were tested, and condition C, under which specimens 1, 2 and 3 were tested were designed to examine the performance of heat exchangers with different geometries under the same frosting conditions. Condition D for specimen 3 was designed for comparison to condition C, in order to assess coolant temperature effects. Condition E for specimen 2 serves as a comparison to condition C for the impact of air flow rate. Furthermore, specimen 2 was tested under condition B. Test 2B in the following text, for example, represents the experiment conducted with specimen 2 under condition B.

Data Reduction

The air-side heat transfer rate is calculated as

$$Q_{air} = Q_{sen} + Q_{latent} \quad (1)$$

$$Q_{sen} = \dot{m}_{air} c_{p,air} \left(T_{air,up} - T_{air,dn} \right) \quad (2)$$

$$Q_{latent} = \dot{m}_{frost} i_{fg} \quad (3)$$

where Q_{sen} is the sensible heat transfer rate, Q_{latent} is the latent heat transfer rate, $\dot{m}_{air}$ is the moist air (that is dry air plus water vapor) mass flow rate, i_{fg} is the enthalpy of freezing evaluated at the tube surface temperature, and $\dot{m}_{frost}$ is the frost accumulation rate, which is calculated from the humidity difference between the upstream and downstream of the test section:

Table1 Geometrical description of the test specimens

Specimen	External Dimensions (H x W x D) (mm^3)	Louver Angle (deg) □	Shape of air flow channel	Total Air-side Surface A_{tot}(m^2)	Louver Pitch Lp
1	406.4 x 381.0 x 15.9	27	rectangular	4.176	1.40
2	406.4 x 381.0 x 27.9	27	triangular	4.079	1.40
3	406.4 x 381.0 x 27.9	27	rectangular	7.370	1.40

Tube Dimensions				Fin dimensions		
Number of Tubes	Wall Thickness □t (mm)	Width Tw (mm)	Depth T_d (mm)	Length FL (mm)	Thickness □mm)	Fin Pitch F_p (mm)
38	0.41	1.88	13.54	7.94	0.18	1.06
38	0.41	1.88	25.40	7.94	0.18	2.12
38	0.41	1.88	25.40	7.94	0.18	1.06

Table 2 Experimental conditions

test condition / **parameter**	**A**	**B**	**C**	**D**	**E**
relative humidity	0.779(±0.024)	0.752(±0.031)	0.776(±0.090)	0.776(±0.070)	0.776(±0.059)
upstream air temperature (□)	1.8(±0.3)	1.8(±0.4)	-8.5 (±0.3)	-8.5 (±0.6)	-8.5 (±0.6)
coolant inlet temperature(□)	-10.4 (±0.4)	-10. 4(±0.2)	-21.5(±0.3)	-25.1(±0.8)	-21.5(±0.4)
coolant mass flow rate (g/s)	105.5(±0.4)	105.5(±0.3)	107.7(±1.2)	107.7(±0.5)	107.7(±0.2)
air flow rate (kg/s)	0.154(±0.002)	0.170(±0.003)	0.157(±0.003)	0.157(±0.003)	0.196(±0.003)
humidity ratio (kg-water/kg-dry air)	0.00336 (±0.00018)	0.00324 (±0.00023)	0.00142 (±0.00021)	0.00142 (±0.00021)	0.00142 (±0.00019)

$$\dot{m}_{frost} = \dot{m}_{air}\left(\frac{\omega_{up}}{1+\omega_{up}} - \frac{\omega_{dn}}{1+\omega_{dn}}\right) \quad (4)$$

where ω_{up} and ω_{dn} are the humidity ratio upstream and downstream of the test section, as determined from the air temperature and the dew-point temperature. The total frost accumulation is calculated by integrating the frost accumulation rate over the time period,

$$m_{frost,tot} = \int_0^t \dot{m}_{frost} dt \quad (5)$$

The frost accumulation from the humidity difference is compared to that from the balance, and the results are within about 15%.

The heat transfer rate to the coolant is

$$Q_c = \dot{m}_c c_{p,c}\left(T_{c,o} - T_{c,i}\right) \quad (6)$$

In order to ensure the fidelity of all measured data, the energy balance is monitored to be always within 10%. For 80% of the measurements, the energy balance is within 5%.

The overall heat transfer coefficient is

$$U = \frac{Q_{sen}}{F \cdot LMTD \cdot A_{tot}} \quad (7)$$

where A_{tot} is the total air-side heat transfer surface including the tube and the fin, F is the correction factor for cross-flow (Incropera *et al*, 1996). The variation of the correction factor is less than 5% during frost growth, and an average value was used in the calculation. LMTD is the log-mean temperature difference defined as

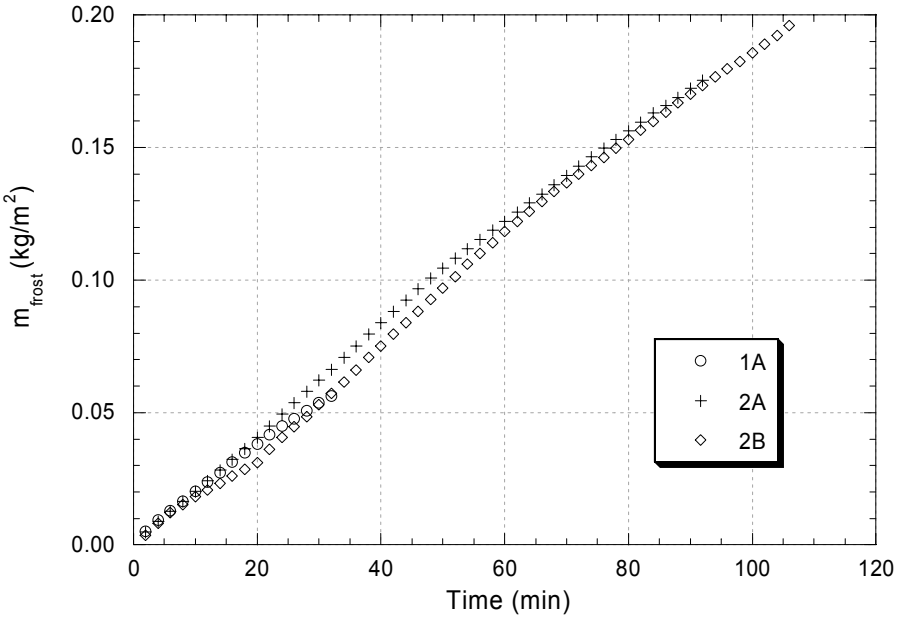

(a)

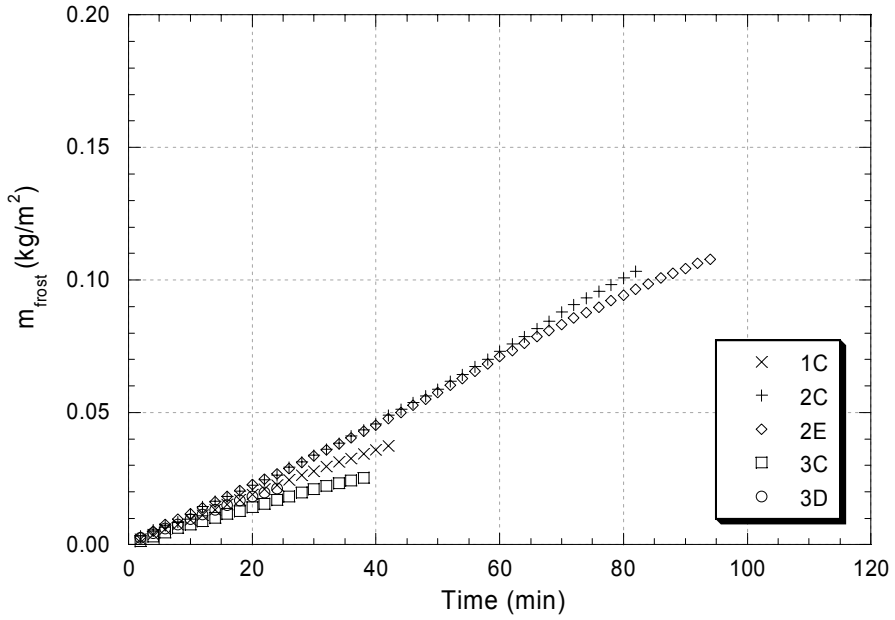

Figure 1 Real-time frost accumulations

$$LMTD = \frac{\left(T_{air,up} - T_{c,o}\right) - \left(T_{air,dn} - T_{c,i}\right)}{\ln\left[\left(T_{air,up} - T_{c,o}\right)/\left(T_{air,dn} - T_{c,i}\right)\right]} \qquad (8)$$

The uncertainty was calculated according to the procedure described in (Taylor *et al.*, 1994). The uncertainty in frost accumulation is less than 13%, the uncertainty in overall heat transfer coefficient is between 3% and 11%.

RESULTS AND DISCUSSION

Frost Accumulation

The variation of frost accumulation on the heat exchanger surface over time is shown in Figure 1. The mass of frost linearly increased over time for all the experiments. Figure 1 shows that the frost accumulation rate, which is defined as the increase in frost mass per unit area, per unit time, remains approximately constant and is highly coupled to operating conditions. The frost accumulation rates during

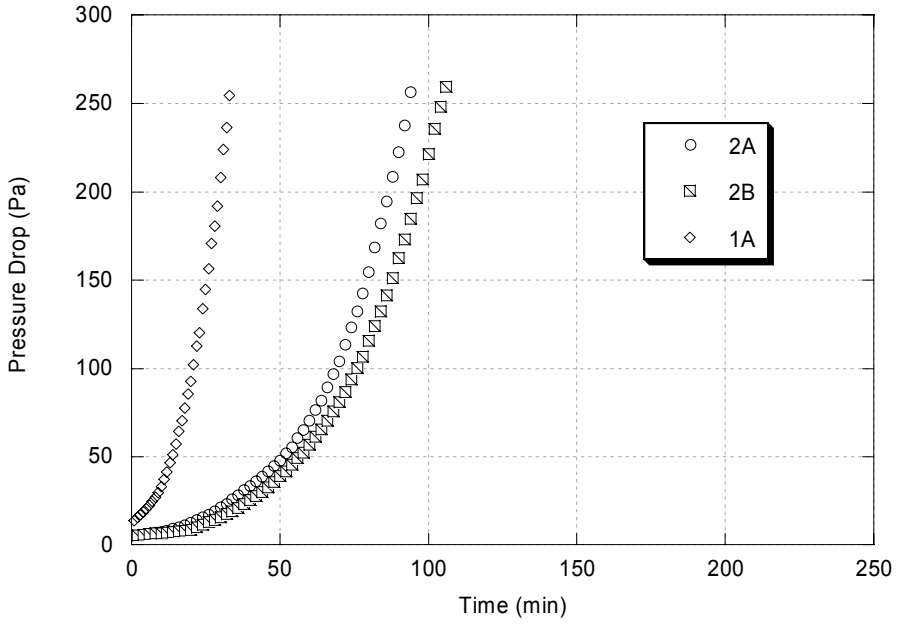

(a)

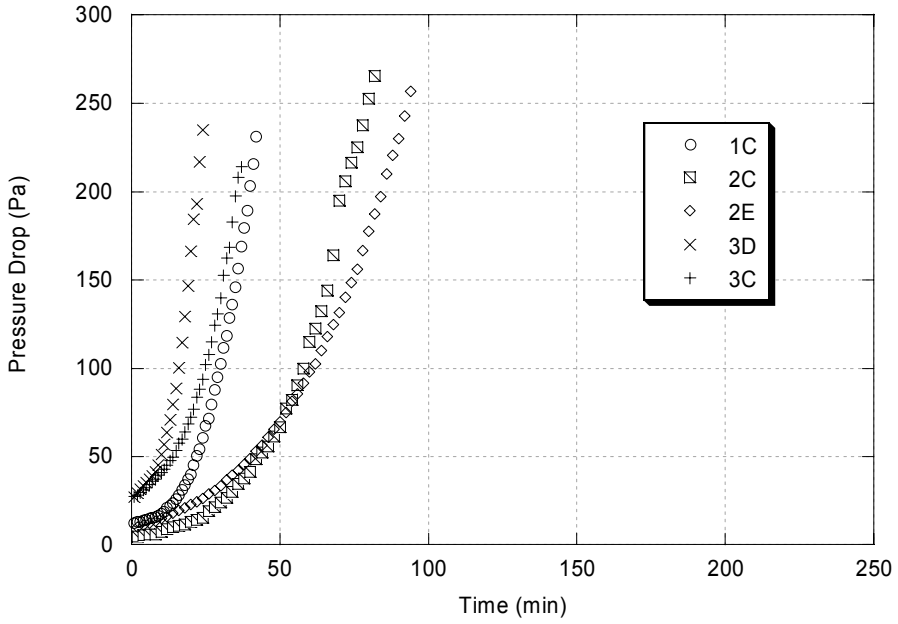

(b)

Figure 2 Real time pressure drops

the experiments conducted under conditions A and B are close to each other as shown in Figure 1(a)—frost accumulation rates are within about 10% during the same test period during test 1A, 2A and 2B. The same situation occurs for the experiments under conditions C, D and E as shown in Figure 1(b). For example, the frost accumulation during test 1C is 0.002 kg/m^2 (18%) smaller than that during test 2C and 2E at the 10th minute, and 0.01 kg/m^2 (23%) at the 42nd minute. On the other hand, the frost accumulation rates in Figure 1(a) are much different from those in Figure 1(b). Thus, the operating conditions control the rate of frost accumulation.

The effects of environmental and geometric parameters can be concluded as following: (1) the air flow rate has little impact on the frost accumulation. A 25% increase in the air mass flow rate led to at most a 3% difference in the frost mass accumulated during the same frost growth period comparing 2E to 2C. Hence, lowering the air flow rate may not be an effective way to mitigate frost growth. (2) The

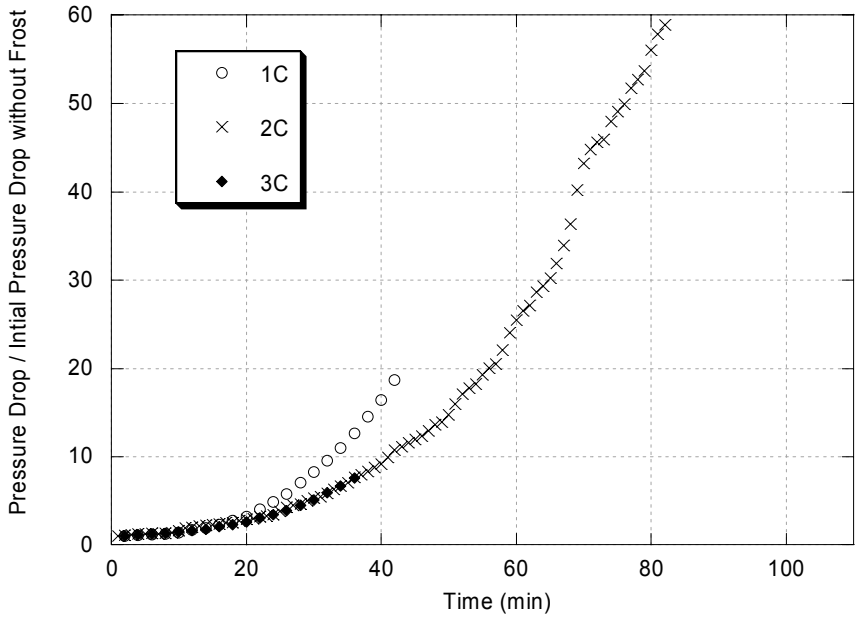

(c)

Figure 2 Real time pressure drops

lower the coolant temperature, the higher the frost accumulation rate. An approximate 30% increase in the frost accumulation rate was found in test 3D as compared to test 3C, due to a 16.5% decrease in the coolant temperature. (3) A small flow depth leads to a fast average frost growth on heat exchanger surface. An 87.6 % increase in flow depth caused an approximate 25% decrease in the frost accumulation rate comparing 3C to 1C. This behavior may be explained by the favored location for frost to grow. Frost readily grows on the edges of fins and louvers instead of the planar parts of fins. Heat exchangers with a large flow depth provide more favored area for frost growth than those with small flow depth. (4) The smaller the fin pitch, the less frost deposits per unit area of surface during the same frost growth period. The frost accumulation rate was about 90% bigger during test 2C than for test 3C, in which the fin pitch of the specimen was 80% smaller.

Pressure Drop

The experimental data on pressure drop across the specimens during frost growth are shown in Figure 2. The geometry of the heat exchanger is the governing factor in pressure drop during frost growth. Firstly, fin pitch dominates the pressure drop behavior during frost growth. Heat exchangers with a small fin pitch tend to have a fast increase in the pressure drop. The pressure drop during the experiments conducted with specimens 1 and 3 was much bigger than with specimen 2 during the same frost accumulation period. The pressure drop during tests 1A, 1C, 3C and 3D increases rapidly throughout the experiments, while the pressure drop during tests 2A, 2B, 2C and 2E increased slowly at the beginning of frost accumulation and then increases quickly. As shown in Figure 2, the average increase in pressure drop during test 1A during the first 15-minute period was 2.7 Pa/minute, and it became 10.0 Pa/minute during the second 15-minute period. In contrast, the average increase in pressure drop during test 2A started at 0.3 Pa/minute during the first 15-minute period, and became 0.8 Pa/minute during the second 15-minute period. At the 30^{th} minute, the pressure drop of test 1A (208.2 Pa) was much higher than the pressure drop of test 2A (21.2 Pa). Another interesting facet of geometric effects on pressure drop is associated with the ratio of the pressure drop during frost growth to the initial pressure drop without frost deposition as shown in Figure 2(c). The ratios during the experiments conducted under condition C were similar during the first 20-minue period. After that period, test 1C (a small flow depth) had a bigger increase in this ratio than the other two tests. This ratio during test 3C was identical to that of test 2C. The specimen used during test 2C has the same flow depth as that during test 3C but an 80% increase in the fin pitch. It seems that flow depth may determine the ratio of the increase in pressure drop.

The effects of environmental parameters on the increase in pressure drop are obtained from the experiments with the same specimen in Figure 2. A fast increase in pressure drop results from a low coolant temperature, as demonstrated by comparing 3D to 3C. The effects of environmental parameters on the pressure drop seem to be closely related to their impacts on frost accumulation—parameters, such as coolant temperature, which tend to increase frost accumulation, have an influence to increase the pressure drop fast. A fast pressure drop during test 2C comparing to test 2E may be due to the large frost accumulation as shown in Figure 1(b).

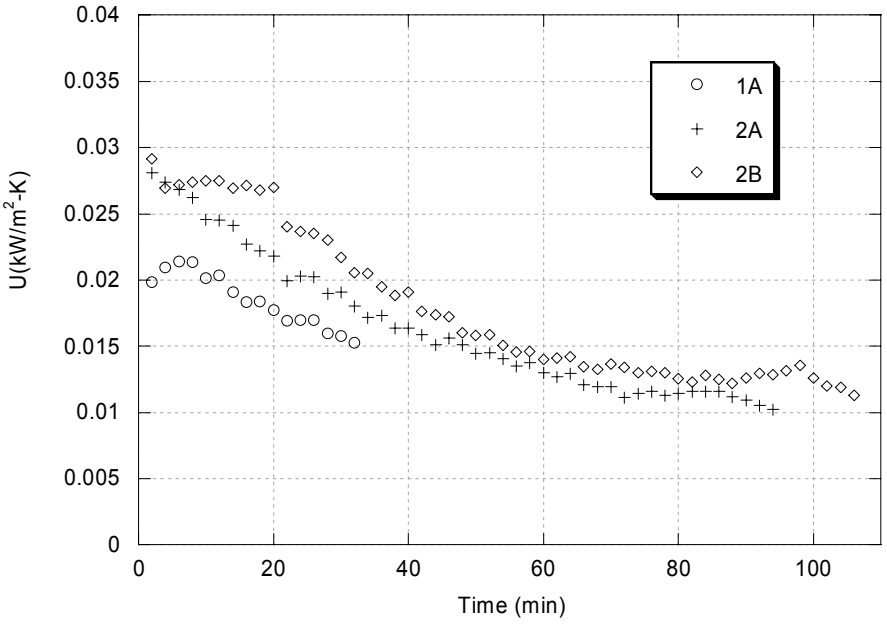

(a)

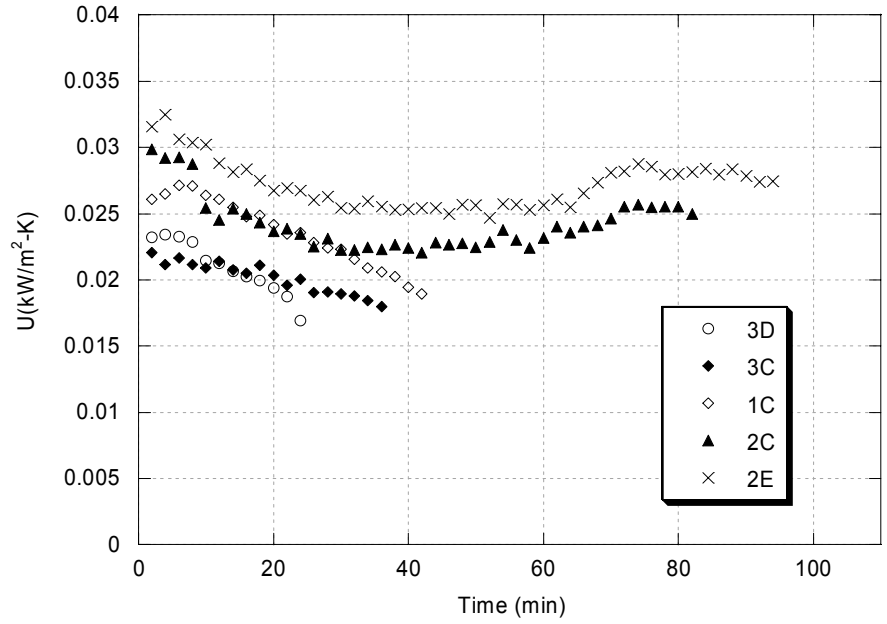

(b)

Figure 3 Real time overall heat transfer coefficients

Overall Heat Transfer Coefficient

The relationship between the overall heat transfer coefficient and frost growth period is shown in Figure 3. The coolant-side heat transfer coefficients are the same for the experiments conducted under the same coolant-side operating conditions, because all the specimens tested in this study have the same tube configuration. Under such conditions, trends in the overall heat transfer coefficient represent changes in the air-side performance caused by frost growth, including both the heat conduction in the frost layer and the convection between the frost surface and the air. Experimental results indicate that the degradation of air-side heat transfer during frost growth has different patterns for different heat exchanger geometries. During all the experiments with specimen 1, the heat transfer coefficients were found to have a slight increase at the beginning of frost growth and then decrease. As for specimen 2, heat transfer coefficients were observed to decrease for some period of frosting and then increase slightly during test 2C and 2E; during test 2A and 2B, heat transfer coefficients

tended to remain almost constant after the declining period. The heat transfer coefficients during the experiments conducted with specimen 3 monotonically decreased. The initial slight increase in heat transfer coefficient could be correlated with the increase in surface roughness due to frost. The increase after some frost growth period could be because the diffusion and solidification of vapor in the frost layer, increase the conductivity of frost. However, our experiments are too limited to know if the conjecture we offer on heat transfer performance is correct.

In some cases, a heat exchanger with a large fin pitch tends to have a high heat transfer coefficient, as shown in Figure 3(b). The heat transfer coefficient during test 2C is always higher than that during 3C, which was conducted with a small fin pitch specimen. Furthermore, the comparison between test 3C and 1C shows that the heat exchanger with a smaller flow depth has a higher heat transfer coefficient during frost growth. This behavior may be because the ratio of developing region to flow depth is larger for the heat exchanger with a smaller flow depth.

Environmental parameters affect the densification and structure of the frost layer as well as the amount of frost deposition, and through those effects impact the overall heat transfer coefficient, which includes conduction in the frost layer and convection between the frost surface and the air. The comparison of heat transfer coefficients during test 2C and 2E shows that the increase in air flow rate improves heat transfer. Approximately a 14% increase in the heat transfer coefficient appeared during test 2E as compared to test 2C at the 30th minute of frost growth. A low coolant temperature during test 3D led to a high heat transfer coefficient at the beginning as compared to test 3C because frost may have a higher density under the low plate temperature, the attendant increase in thermal conductivity is manifested as an increase in the overall heat transfer coefficient. However, a low coolant temperature also resulted in a large rate of frost accumulation which caused a rapid degradation of the overall heat transfer coefficient.

CONCLUSION

An experimental study on the performance of louver-fin flat-tube heat exchangers under the frosting conditions is presented in this paper to examine these effects over a broad range of operating conditions. The increase in frost accumulation is a strong function of the operating conditions. The trends in pressure drop are dominated by the fin pitch during frost growth. One very interesting result is that the ratio of the pressure drop during frost growth to the initial pressure drop without frost was found to be the same for the heat exchangers with the same air flow depth but different fin pitches. For the operating ranges studied, a low coolant temperature, a large air flow depth or a small fin pitch leads to a large frost accumulation rate and a fast increase in pressure drop.

The overall air-side heat transfer coefficients show very different trends in heat transfer degradation for heat exchangers with different geometries. The heat exchanger with the largest fin pitch had a large overall heat transfer coefficient. A small flow depth results a high overall heat transfer coefficient, caused by flow development effects. A large air flow rate tends to increase heat transfer coefficient. Conduction in the frost layer may be affected greatly by coolant temperature, and vapor diffusion during frost growth.

The experiments used to draw these conclusions are limited, both in specimen geometry and operating range. Perhaps the most important limitations are related to coolant temperature and flow rates and air humidity and flow rates. These factors have an obvious and profound effect on frost distribution across the face and along the depth of the heat exchanger. Frost distribution can have a profound impact on air-flow distribution, pressure drop and heat transfer.

ACKNOLEDGMENTS

This work was financially supported by the Air-Conditioning and Refrigeration Technology Institute (ARTI) under 21-CR, Elizabeth Jones program director, and by the Air-Conditioning and Refrigeration Center. Their support is gratefully acknowledged.

REFERENCES

Webb RL. 1994, Principles of Enhanced Heat Transfer. John Willey & Sons Inc..

Kim JH, Groll EA. 2003, Performance comparisons of a unitary split system using microchannel and fin-tube outdoor coils. ASHRAE Trans. 109(2):219-229.

Xia Y., Hrnjak P.S., Jacobi A.M., 2004, An empirical study of frost accumulation effects on louvered-fin, microchannel heat exchangers. International Refrigeration and Air Conditioning Conference at Purdue, July 12-15.

Lee K.S., Kim W.S., Lee T.H., A one-dimensional model for frost formation on a cold flat surface,1997. Int. J. Heat and Mass Transfer, 40(18):4359-4365.

Xia Y., Hrnjak P.S., Jacobi A.M., 2005, The air-side thermal-hydraulic performance of louvered-fin, flat-tube heat exchangers with sequential frost-growth cycles. Accepted by ASHRAE Trans., part(1).

Joardar A., Gu Z., Jacobi A.M., 2004, Accessing the condensate drainage behavior of dehumidifying heat exchangers. International Refrigeration and Air Conditioning Conference at Purdue, July 12-15.

Incropera FP, DeWitt DP. 1996, Fundamentals of Heat and Mass Transfer, 4th edition. John Wiley & Sons Inc.

Taylor B.N., Kuyatt C.E., 1994, Guidelines for Evaluating and Expressing the Uncertainty of NIST Measurement Results, National Institute of Standards and Technology Technical Note 1297.